第 27 卷 第 2 期
2021 年 4 月

电化学
JOURNAL OF ELECTROCHEMISTRY

Vol. 27 No. 2
Apr. 2021

【Article】 **DOI**: 10.13208/j.electrochem.201248 **Http**://electrochem.xmu.edu.cn

Theoretical Studies of Metal-N-C for Oxygen Reduction and Hydrogen Evolution Reactions in Acid and Alkaline Solutions

Xue-Ping Qin[1*], Shang-Qian Zhu[1], Lu-Lu Zhang[1],
Shu-Hui Sun[2], Min-Hua Shao[1*]

(1. *Department of Chemical and Biological Engineering, The Hong Kong University of Science and Technology, Clear Water Bay, Kowloon, Hong Kong 999077, China*; 2. *INRS-Énergie, Matériaux et Télécommunications, 1650 Boulevard Lionel Boulet, Varennes, Québec, Canada J3X 1S2*)

Abstract: Single atom catalysts (SAC) have been regarded as the promising alternatives to platinum group metals due to their low costs and potentially high catalytic activities in various electrocatalytic reactions. The atomic mechanism understanding of activity discrepancy among different metal and nitrogen co-doped carbon-based catalysts is still lacking. Here, non-precious metal and nitrogen co-doped carbons (Me-N-C, Me = Fe and Co) as the model catalysts are investigated by combining experimental and theoretical studies to explore the catalytic activities and corresponding reaction mechanisms toward oxygen reduction reaction (ORR) and hydrogen evolution reaction (HER) at universal pHs. Atomic theoretical simulations suggest that Fe-N-C has higher ORR activity than Co-N-C due to its lower reaction barrier of the rate-determining step, while the activity trend is reversed for HER. Our simulation results are consistent with experimental observations.

Key words: oxygen reduction reaction; hydrogen evolution reaction; electrocatalysts; single atom catalysts; theoretical calculations

1 Introduction

Platinum group metals (PGMs) are generally efficient catalysts for many electrocatalytic reactions, but high cost and stability issue prohibit their wide applications and practical scaling up[1-4]. Numerous efforts have been devoted into developing non-precious-metal-based catalysts, such as transition-metal-based compounds including carbides[5], nitrides[6] and sulfides [7]. During the development of PGM-free electrocatalysts for both polymer electrolyte membrane fuel cells and electrolyzers, non-precious metal and nitrogen co-doped carbon (Me-N-C) or single metal catalyst (SAC) has been widely investigated as a promising catalyst for oxygen reduction reaction (ORR)[8-12] and hydrogen evolution reaction (HER)[13, 14]. However, these studies were conducted by different groups under various experimental conditions, where the lateral comparisons cannot be made to obtain the general trend and the systematic understanding toward catalytic activities. Most of the experiments were focused on a certain kind of reaction (ORR or HER) in either acid or alkaline media. Additionally, current understanding cannot explain well the activity discrepancy between Fe-N-C and Co-N-C. For instance, the former is much more active than the latter toward ORR, while the trend is reversed for HER[13]. Moreover, Co-N-C was synthesized and regarded as the efficient electrocatalyst for ORR as discussed in

Citation: Qin X P, Zhu S Q, Zhang L L, Sun S H, Shao M H. Theoretical studies of metal-N-C for oxygen reduction and hydrogen evolution reactions in acid and alkaline solutions. *J. Electrochem.*, 2021, 27(2): 185-194.

Received: 2021-02-02, Revised: 2021-03-10. *Corresponding author, Tel: (86-852)34692269, Fax: (86-852)23580054, E-mail: kemshao@ust.hk; xqinaa@connect.ust.hk

previous studies[15-17], while Fe-N-C was also claimed to be good ORR catalyst with high performance and can be applied in direct methanol fuel cell[18]. Another experiment conducted by Wang et al. also demonstrated that Fe-N-C showed excellent ORR activity and Co-N-C exhibited high HER activity, thus contributing to the remarkable ORR and HER performances in the Fe/Co decorated nitrogen doped carbon[19]. Therefore, it is necessary to conduct a systematic study on Me-N-C using Fe-N-C and Co-N-C as the model electrocatalysts for ORR and HER at universal pHs.

In this study, the model catalysts Fe-N-C and Co-N-C were synthesized using metal organic frameworks (Me-MOFs) as templates. Their catalytic activities of ORR and HER were evaluated in both acid and alkaline media, respectively. The performance measurements indicated that Fe-N-C was better for ORR than Co-N-C but not for HER at universal pHs. The discrepancy of activity trend is further explained and supported by density functional theory (DFT) calculations, where the reaction mechanisms of ORR and HER on these two model catalysts are explored at the atomic level. The theoretical simulation results demonstrated that Fe-N-C shows a higher ORR activity than Co-N-C by reducing the reaction barrier of the rate-determining step (RDS), while a completely different trend is observed for HER where Co-N-C has smaller reaction barriers of RDS in both acidic and alkaline media.

2 Experimental Section

2.1 Electrochemical Performance Measurements

In this work, two types of Me-N-C (Me = Fe and Co) catalysts derived from metal organic framework (MOF) were evaluated for ORR and HER in both acid and alkaline media. The detailed synthesis protocols and characterizations of the Me-N-C catalysts can be found in previous reports[20, 21].

Typically, 10 mg of the synthesized Me-N-C catalyst was dispersed in a solution consisting of 4 mL of ultrapure water (Merck Millipore), 1 mL of isopropanol (99.9% Sigma-Aldrich), and 20 μL of Nafion 117 solution (5wt.%, Sigma-Aldrich) via sonication for 30 min to form a homogeneous ink, which was then loaded and dried on a pre-polished glassy carbon rotation disk electrode (GC-RDE, 5 mm, Pine Instruments) with a desired loading amount. All the electrochemical measurements were conducted in a typical three-electrode setup with a pre-calibrated Ag/AgCl and Hg/HgO electrodes used as the reference electrodes in acid and alkaline solutions, respectively. A graphite rod was used as the counter electrode. All potentials were referred to a reversible hydrogen electrode (RHE). The potential was controlled by a CHI627e or CHI760e electrochemical workstation (CH Instruments). The HER performance was recorded by linearly sweeping the working electrode potential from 0.1 V to negative potentials at a scanning rate of 10 $mV \cdot s^{-1}$ in an Ar-saturated 0.5 $mol \cdot L^{-1}$ H_2SO_4 (Veritas double distilled from VYCOR, GFS Chemicals) or 1 $mol \cdot L^{-1}$ KOH solution (99.99% Aladdin). The working electrode was not rotated in HER performance evaluation. ORR polarization curves were recorded in O_2-staturated solutions (0.1 $mol \cdot L^{-1}$ $HClO_4$ (Veritas double distilled, GFS Chemicals) or KOH) with the steady-state mode consisting of a potential step of 25 mV (between 0.40 and 0.95 V vs. RHE) and step duration of 30 s at a rotation speed of 1600 $r \cdot min^{-1}$.

2.2 Computational Methods

Density functional theory (DFT) calculations are conducted to compare the catalytic activity differences between Fe-N-C and Co-N-C by exploring the ORR and HER mechanisms in both acid and alkaline solutions. Vienna Ab-initio Simulations Package (VASP)[22, 23] is adopted using the projected augmented wave (PAW)[24, 25] method with the periodic boundary condition being considered. The generalized gradient approximation (GGA) is used to evaluate the electronic exchange-correlation energies by adopting the revised Perdew-Burke-Ernzerhof (RPBE)[26] functional during calculations. The cut-off energy is set to be 400 eV, and the conjugate-gradient scheme is used to carry out the ionic relaxations under the force criterion of 0.02 $eV \cdot Å^{-1}$. The energy convergence criteri-

on is 1×10^{-6} eV, and one vacuum layer of 20 Å is added along z axis to avoid periodic interactions. Spin polarizations are considered.

To investigate the ORR and HER activities on Me-N-C catalyst surfaces theoretically, Fe-N-C and Co-N-C are used as model catalysts to simulate the elementary reaction steps. (6×6) supercell is built with the embedded Me-N_4 moiety being the active site. The Monkhorst-pack ($2 \times 2 \times 1$) grid is used to sample the Brillouin zone for the modelled Me-N-C[27]. Both the explicit and implicit solvent models are included into our simulations to consider the solvation effect, which is illustrated to be critical to explore the interfacial reaction mechanisms[28-30]. For the explicit solvation effect, one water bilayer is used with a planar hexagonal hydrogen bond network, where one half of water molecules point to the slab by hydrogens and the other half lie parallel to the catalyst surfaces[30-32]. For the implicit solvation effect, the solvation model developed by Hennig's group is introduced treating the solvent as a continuum described by certain dielectric constant, which follows the joint density functional theory framework[33, 34]. Such a similar theoretical model has been applied into other electrochemical systems[35, 36]. Gibbs free energy diagrams of ORR and HER in both acid and alkaline solutions were constructed according to Nørskov's method[37]. The free energy during all the elementary steps is calculated as:

$$\Delta G = \Delta E + \Delta E_{ZPE} - T\Delta S$$

where the ΔE is the DFT-calculated reaction energy, ΔE_{ZPE} is the zero-point correction energy and $T\Delta S$ is the entropy term. The ΔE_{ZPE} can be obtained by the harmonic vibrational frequency calculations. By including the water layer explicitly, the binding energy of adsorbates can be calculated using the equation:

$$\Delta E = E_{total} - E_{(slab+water)} - E_{adsorbate}$$

where E_{total} includes the DFT-calculated total energy of slab and water layer, as well as adsorbate. Since the interaction energy between water and Me-N-C exists in all of the intermediate structures, it can be counteracted during Gibbs free energy change (ΔG) evaluations. The reaction pathways are searched by the climbing image nudged elastic band (CINEB) method[38-40] and the reaction barrier is calculated as the energy difference between the reactant and transition state.

3 Results and Discussion

3.1 Experimental Measurements of ORR and HER Performances on Me-N-C at Universal pHs

To understand the impact of metal centers on catalytic performances of Me-N-C, their ORR and HER performances in both acid and alkaline environments were evaluated. As shown in Figure 1A, the Fe-N-C catalyst exhibited a half-wave potential ($E_{half\text{-}wave}$) of 0.766 V vs. RHE in acid media toward ORR, which was much higher than that of Co-N-C ($E_{half\text{-}wave}$ = 0.731 V), demonstrating the faster reaction kinetics on the former. The much better ORR performance of Fe-N-C than that of Co-N-C was also observed in alkaline media (Figure 1B, $E_{half\text{-}wave}$: Fe-N-C (0.900 V) > Co-N-C (0.857 V)). These results demonstrated that Fe center has much faster kinetics in catalyzing ORR than the Co one in both acid and alkaline media. It should also be noted that Fe-N-C exhibited obviously larger mass transport limiting current densities in both acid and alkaline environments, suggesting that it was more superior in catalyzing the complete reduction of O_2 to H_2O ($4e^-$ pathway). The HER activities of these two catalysts were also evaluated. At a geometric current density of 10 mA·cm^{-2} (Figure 1C) in acid media, the HER overpotential measured on Co-N-C was 240 mV, which was significantly smaller than that on Fe-N-C (434 mV) by ca. 200 mV, illustrating the far higher HER activity and faster reaction kinetics on the Co-doped carbon catalyst. Similarly, in alkaline media as shown in Figure 1D, the same overpotential sequence at the current density of 10 mA·cm^{-2} was obtained (Co-N-C (260 mV) < Fe-N-C (360 mV)). Therefore, contrary to the above observed ORR activity trend, Co-N-C showed much higher activity toward HER than Fe-N-C at universal pHs.

3.2 ORR Mechanisms on Me-N-C at Universal pHs

To explore the origin of electrocatalytic activity

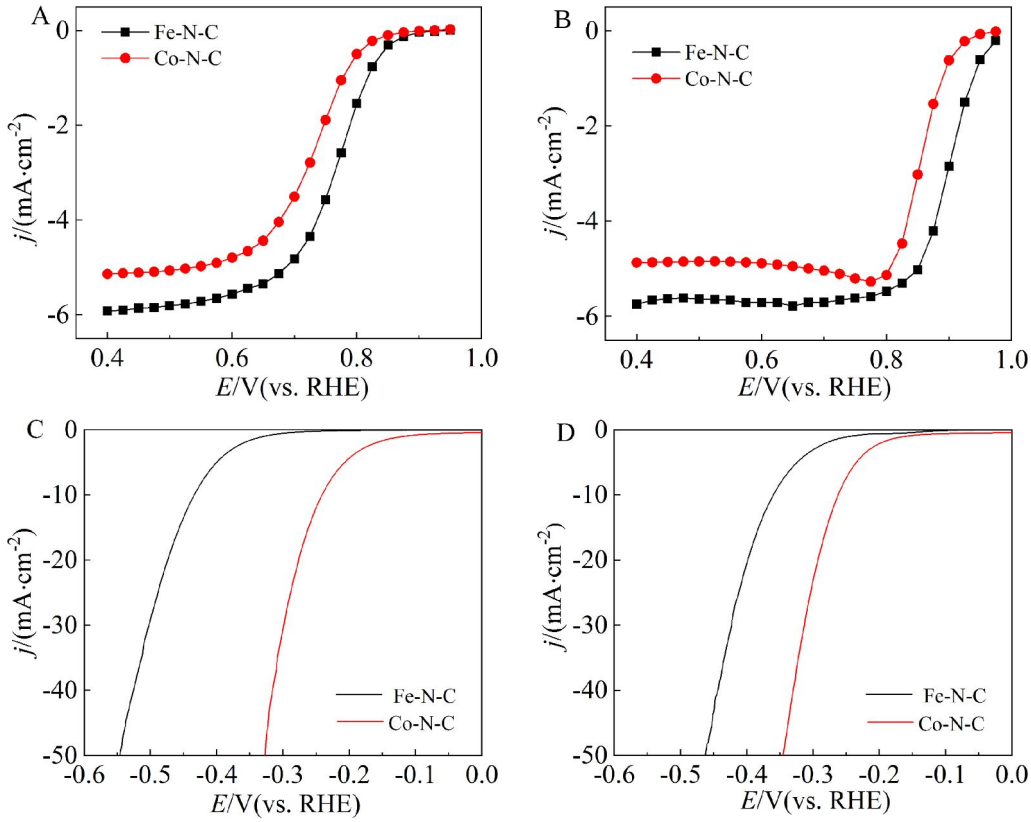

Figure 1 Steady-state ORR polarization curves of Fe-N-C and Co-N-C in O_2-saturated 0.1 mol·L^{-1} $HClO_4$ (A) and 0.1 mol·L^{-1} KOH (B) solutions. The catalyst loading was 306 μg·cm^{-2}. The RDE rotation speed was 1600 r·min^{-1}. Polarization curves of Fe-N-C and Co-N-C in Ar-saturated 0.5 mol·L^{-1} H_2SO_4 (C) and 1 mol·L^{-1} KOH (D) solutions at a scanning rate of 10 mV·s^{-1}. The catalyst loading was 255 μg·cm^{-2}. (color on line)

discrepancy between Fe-N-C and Co-N-C, DFT simulations are conducted to study the reaction mechanisms during ORR on Fe-N-C and Co-N-C in both acid and alkaline solutions. The ORR mechanism has been previously reported to be the four-electron reaction pathway on Me-N-C at universal pHs[32, 41, 42]. The main difference in acid and alkaline solutions is the origin of protons, which means that protons directly come from the hydronium ($H_3O^+ \cdot (H_2O)_n$) in acid media, while from water dissociations in alkaline solutions. Since the liquid environment influenced the electrocatalytic reactions greatly at the solid-liquid interface[30, 43, 44], one water bilayer (explicit solvation) and implicit solvation model are introduced into the simulation system, representing the interfacial area and bulk region, respectively. The reac tion pathways are shown and discussed in the following sections.

In acid,

$$* + O_2 + H^+ + e^- \rightarrow *OOH \quad (1)$$

$$*OOH + H^+ + e^- \rightarrow *O + H_2O \quad (2)$$

$$*O + H^+ + e^- \rightarrow *OH \quad (3)$$

$$*OH + H^+ + e^- \rightarrow * + H_2O \quad (4)$$

As stated in the above discussion, H^+ is in the form of hydronium represented by $H_3O^+ \cdot (H_2O)_n$. The adsorption structures of key intermediates (i.e., *OOH, *O and *OH) on Fe-N-C during ORR are optimized as shown in Figure 2 and the corresponding structures on Co-N-C are similar but with different metal centers in the $Me-N_4$ species. After geometry optimizations, *OOH, *O and *OH on the active metal site all have the weak hydrogen bonds between adsorbates and water bilayers indicated by the black dashed lines as shown in Figure 2, where the local rearrangements of water network are observed once the reaction intermediates are adsorbed on Fe-N-C. Cor-

respondingly, the Gibbs free energy diagrams of ORR on both Fe-N-C and Co-N-C in acid media are constructed (Figure 3A), where the four elementary steps are all in the downhill trend on these two catalyst surfaces, demonstrating the facile reaction process from the thermodynamic aspect. Moreover, the kinetic barriers are also evaluated by searching the minimum energy path (MEP) and transition state (TS). Our calculation results indicate that the continuous hydrogenation steps including O_2-to-*OOH (Eq.1), *O-to-*OH (Eq. 3) and *OH-to-*H_2O (Eq. 4) are facile and barrierless except the *OOH-to-*O (Eq. 2) conversion step, which requires the O-O bond cleavage in *OOH species. The reaction barriers of *OOH-to-*O step on Fe-N-C and Co-N-C are marked in Figure 3A by E_a, and apparently, Fe-N-C can facilitate the *OOH-to-*O conversion being the rate-determining step (RDS) with a much lower barrier of 0.19 eV compared to that on Co-N-C (0.61 eV). These results well explain why Fe-N-C exhibits a higher ORR activity in acid than Co-N-C.

The ORR pathways in alkaline solutions are also explored on Me-N-C, and the four elementary reaction steps are shown below:

In alkaline,

$$* + O_2 + H_2O + e^- \rightarrow *OOH + OH^- \quad (5)$$

$$*OOH + e^- \rightarrow *O + OH^- \quad (6)$$

$$*O + H_2O + e^- \rightarrow *OH + OH^- \quad (7)$$

$$*OH + e^- \rightarrow * + OH^- \quad (8)$$

The Gibbs free energy diagrams of ORR in alkaline are shown in Figure 3B, and the reaction barriers of elementary steps are calculated and shown by the

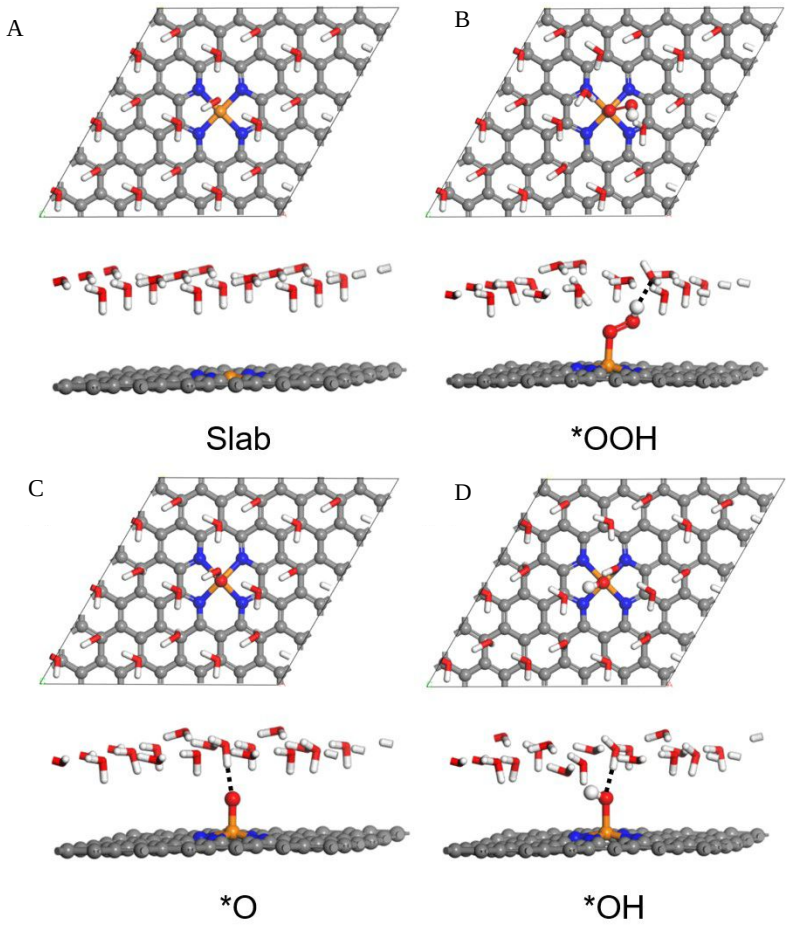

Figure 2 Top view and side view of slab model and adsorption structures of reaction intermediates during ORR on Fe-N-C: (A) slab model; (B) *OOH; (C) *O; (D) *OH. Black dashed lines in B, C and D show the weak hydrogen bonds between adsorbates and water bilayers. Reaction intermediates (*OOH, *O and *OH) are shown in ball-and-stick mode, and water molecules in the bilayer are shown in stick mode. Color code: Fe, orange; C, grey; N, dark blue; O, red; H, white. (color on line)

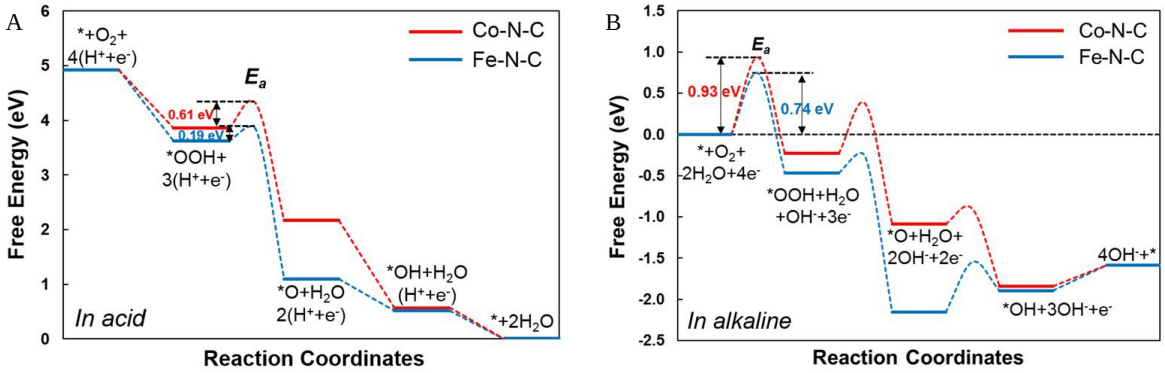

Figure 3 Gibbs free energy diagrams for ORR on Fe-N-C and Co-N-C in acid (A) and alkaline (B) solutions (color on line)

dashed lines. Different from acid, the proton source from water dissociations contributes to the activation energies for the hydrogenation steps during ORR in alkaline, and the initial *OOH formation step is the RDS on both Fe-N-C and Co-N-C (marked as E_a in Figure 3B). By comparing the thermodynamic trend and kinetics barriers, Fe-N-C shows better ORR activity in alkaline with a lower barrier of 0.74 eV in the *OOH formation step (Eq. 5) than Co-N-C (barrier = 0.93 eV), which controls the overall reaction rate and contributes to the faster kinetics. The optimized geometries of reactant, TS and product in the rate-determining *OOH formation step and the corresponding energy curves along with TS searching on Fe-N-C and Co-N-C are shown in Figure 4, where the proton transfer processes are indicated by the yellow atoms and black dashed lines. Based on the above discussion, similar to acid, Fe-N-C can facilitate ORR in alkaline by accelerating the reaction kinetics with the reduced reaction barrier of the RDS compared to Co-N-C.

3.3 HER Mechanisms on Me-N-C at Universal pHs

To explore the HER pathway and to compare the electrocatalytic activities on Fe-N-C and Co-N-C theoretically, the three-stage diagram (ΔG_H^*) is constructed (Figure 5A) and the optimized *H adsorption structures are shown in Figure 5B and 5C. Theoretical calculation results show that Co-N-C with much stronger binding to *H results in the ΔG_H^* of 0.06 eV, which is much closer to 0 than that on Fe-N-C (0.35 eV). Generally, the ΔG_H^* closer to 0 can contribute to better HER activity according to the Sabatier principle. Therefore, thermodynamically, Co-N-C should have a higher activity than Fe-N-C. Afterwards, to analyze the kinetics of HER, the reaction steps including Volmer and Heyrovsky steps are simulated on both metal active sites, and the Tafel step consisting of two adsorbed *H in the combination step is ignored since there is only one metal site in the Me-N moiety. Based on the TS searching and energy barrier calculations (Table 1), HER in acid proceeds on both Co-N-C and Fe-N-C fast with the Heyrovsky step being the RDS, and the corresponding barrier is smaller on Co-N-C (0.25 eV) than that on Fe-N-C (0.29 eV). However, in alkaline, the Volmer step is RDS, and Co-N-C still shows a smaller kinetic barrier of 1.62 eV compared to Fe-N-C (1.95 eV). Therefore, contrary to the trend in ORR, Co-N-C leads to a higher catalytic activity toward HER than Fe-N-C at universal pHs from both thermodynamic and kinetic aspects, which is consistent with the above experimental measurements.

3.4 Model Discussion

Based on the above results, the activity difference of ORR between Fe-N-C and Co-N-C originates from the reaction kinetics in the RDS, where Fe-N-C facilitates ORR in both acid and alkaline solutions compared to Co-N-C, and therefore, contributes to a higher ORR activity at universal pHs. It should be noted that ORR activity in alkaline is better than that in acid on Me-N-C from the experimental measure-

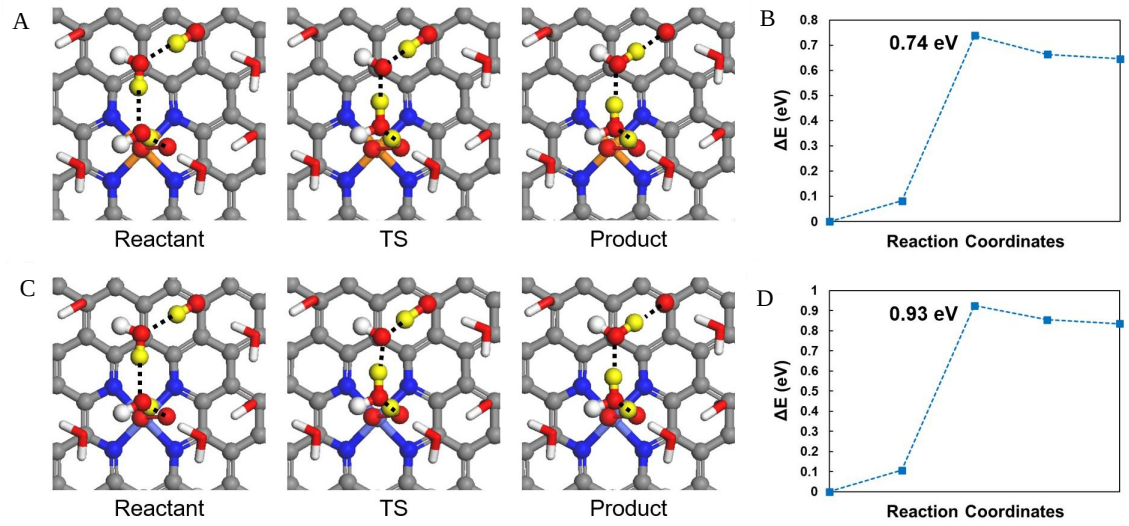

Figure 4 Optimized geometries of reactant, transition state (TS) and product in the rate-determining *OOH formation step during ORR in alkaline media and the corresponding energy curves along with TS searching on Fe-N-C (A, B) and Co-N-C (C, D). The black dashed line (B and C) indicates the proton transfer pathway, and the transferred protons are shown in the yellow balls. The involved water molecules and adsorbed intermediates are shown in ball-and-stick mode, and other water molecules are in stick mode for clarity. Color code: Fe, orange; Co, light blue; C, grey; N, dark blue; O, red; H, white. (color on line)

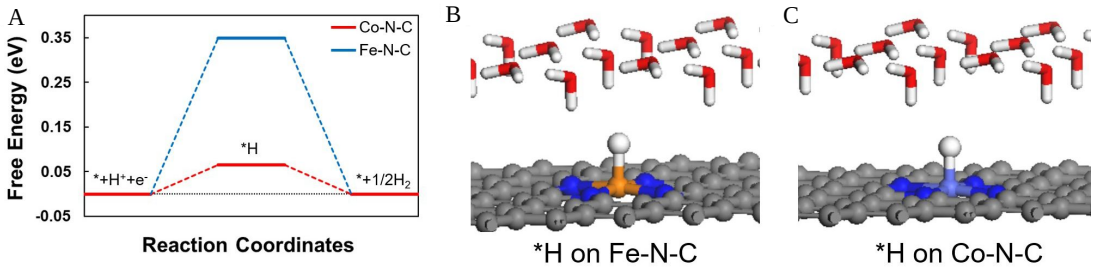

Figure 5 (A) Gibbs free energy diagrams of $\Delta G(H^*)$ for HER on Fe-N-C and Co-N-C; *H adsorption structures on Fe-N-C (B) and Co-N-C (C). Water molecules are shown in stick mode for clarity. Color code: Fe, orange; Co, light blue; C, grey; N, dark blue; O, red; H, white. (color on line)

Table 1 Reaction barriers for HER (E_a) on Fe-N-C and Co-N-C in acid and alkaline solutions. The reaction barriers in RDS are shown in bold.

E_a/eV	In acid		In alkaline	
	Fe-N-C	Co-N-C	Fe-N-C	Co-N-C
Volmer step	0.24	0.09	**1.95**	**1.62**
Heyrovsky step	**0.29**	**0.25**	1.46	1.46

ments, while our simulation results show a higher reaction barrier in RDS in an alkaline medium compared to the acid one. The similar phenomenon is observed for HER on Fe-N-C with higher catalytic activity in an alkaline medium. The high energy barrier in alkaline solutions originates from the water dissociations, and it could be affected by nearby cations at electrochemical interfaces, where multiple water layers and applied potential should also be included in the theoretical models. It is predicted that the simulation models can be expanded and modified to include the complex water network and cations/anions, as

well as the potential effect, which deserves further study and will be included in the future work.

4 Conclusions

In this work, both ORR and HER mechanisms at universal pHs are studied on Fe-N-C and Co-N-C by theoretical simulations from the atomic level. By exploring the reaction pathways, Fe-N-C facilitates ORR in acid and alkaline media by lowering the reaction barriers of RDS compared to Co-N-C. Regarding HER, however, Co-N-C contributes to the higher catalytic activity from both thermodynamic and kinetic aspects than Fe-N-C. Overall, our combined experimental and theoretical studies demonstrated that Fe-N-C had higher ORR but lower HER activities than Co-N-C in both acid and alkaline media.

Acknowledgements

This work was supported by Research Grant Council (C6011-20G, 16308420, and N_HKUST610/17) of the Hong Kong Special Administrative Region. S.Z wishes to thank the support from the Research Grants Council Postdoctoral Fellowship Scheme (PDFS2021-6S08). The Tianhe-2 National Supercomputer Center in Guangzhou and high-performance computing service in HKUST are highly acknowledged.

References:

[1] Xia B Y, Yan Y, Li N, Wu H B, Lou X W, Wang X. A metal-organic framework-derived bifunctional oxygen electrocatalyst[J]. Nat. Energy, 2016, 1(1): 15006.

[2] Ma T Y, Ran J, Dai S, Jaroniec M, Qiao S Z. Phosphorus-doped graphitic carbon nitrides grown *in situ* on carbon-fiber paper: Flexible and reversible oxygen electrodes [J]. Angew. Chem. Int. Ed., 2015, 54(15): 4646-4650.

[3] Gong K P, Du F, Xia Z H, Durstock M, Dai L M. Nitrogen-doped carbon nanotube arrays with high electrocatalytic activity for oxygen reduction[J]. Science, 2009, 323 (5915): 760-764.

[4] Liang Y Y, Li Y G, Wang H L, Zhou J G, Wang J, Regier T, Dai H J. Co_3O_4 nanocrystals on graphene as a synergistic catalyst for oxygen reduction reaction[J]. Nat. Mater., 2011, 10(10): 780-786.

[5] Michalsky R, Zhang Y J, Peterson A A. Trends in the hydrogen evolution activity of metal carbide catalysts[J]. ACS Catal., 2014, 4(5): 1274-1278.

[6] Cao B, Veith G M, Neuefeind J C, Adzic R R, Khalifah P G. Mixed close-packed cobalt molybdenum nitrides as non-noble metal electrocatalysts for the hydrogen evolution reaction[J]. J. Am. Chem. Soc., 2013, 135(51): 19186-19192.

[7] Wang H T, Lu Z Y, Xu S C, Kong D S, Cha J J, Zheng G Y, Hsu P C, Yan K, Bradshaw D, Prinz F B, Cui Y. Electrochemical tuning of vertically aligned MoS_2 nanofilms and its application in improving hydrogen evolution reaction[J]. Proc. Natl. Acad. Sci., 2013, 110(49): 19701-19706.

[8] Wu G, More K L, Johnston C M, Zelenay P. High-performance electrocatalysts for oxygen reduction derived from polyaniline, iron, and cobalt[J]. Science, 2011, 332(6028): 443-447.

[9] Shao M H, Chang Q W, Dodelet J P, Chenitz R. Recent advances in electrocatalysts for oxygen reduction reaction [J]. Chem. Rev., 2016, 116(6): 3594-3657.

[10] Lefèvre M, Proietti E, Jaouen F, Dodelet J P. Iron-based catalysts with improved oxygen reduction activity in polymer electrolyte fuel cells[J]. Science, 2009, 324(5923): 71-74.

[11] Zhang Y F(张焰峰), Xiao F(肖菲), Chen G Y(陈广宇), Shao M H(邵敏华). Fuel cell performance of non-precious metal based electrocatalysts[J]. J. Electrochem.(电化学), 2020, 26(4): 563-572.

[12] Xiu L Y(修陆洋), Yu M Z(于梦舟), Yang P J(杨鹏举), Wang Z Y(王治宇), Qiu J S(邱介山). Caging porous Co-NC nanocomposites in 3D graphene as active and aggregation-resistant electrocatalyst for oxygen reduction reaction[J]. J. Electrochem.(电化学), 2018, 24(6): 715-725.

[13] Zhang L L, Liu W, Dou Y B, Du Z, Shao M H. The role of transition metal and nitrogen in metal-N-C composites for hydrogen evolution reaction at universal pHs[J]. J. Phys. Chem. C, 2016, 120(51): 29047-29053.

[14] Shahraei A, Moradabadi A, Martinaiou I, Lauterbach S, Klemenz S, Dolique S, Kleebe H J, Kaghazchi P, Kramm U I. Elucidating the origin of hydrogen evolution reaction activity in mono- and bimetallic metal- and nitrogen-doped carbon catalysts (Me-N-C)[J]. ACS Appl. Mater. Interfaces, 2017, 9(30): 25184-25193.

[15] Zhu Z J, Chen C M, Cai M Q, Cai Y, Ju H X, Hu S W, Zhang M. Porous Co-N-C ORR catalysts of high performance synthesized with ZIF-67 templates[J]. Mater. Res. Bull., 2019, 114: 161-169.

[16] Chen L Y, Liu X F, Zheng L R, Li Y C, Guo X, Wan X, Liu Q T, Shang J X, Shui J L. Insights into the role of active site density in the fuel cell performance of Co-N-C catalysts[J]. Appl. Catal. B Environ., 2019, 256: 117849.

[17] Ai K L, Li Z L, Cui X Q. Scalable preparation of sized-

controlled Co-N-Celectrocatalyst for efficient oxygen reduction reaction[J]. J. Power Sources, 2017, 368: 46-56.

[18] Sebastián D, Serov A, Artyushkova K, Gordon J, Atanassov P, Aricò A S, Baglio V. High performance and cost-effective direct methanol fuel cells: Fe-NC methanol-tolerant oxygen reduction reaction catalysts[J]. ChemSusChem, 2016, 9(15): 1986-1995.

[19] Wang Y, Pan Y, Zhu L K, Yu H H, Duan B Y, Wang R W, Zhang Z T, Qiu S L. Solvent-free assembly of Co/Fe-containing MOFs derived N-doped mesoporous carbon nanosheets for ORR and HER[J]. Carbon, 2019, 146: 671-679.

[20] Zhang G X, Chenitz R, Lefèvre M, Sun S, Dodelet J P. Is iron involved in the lack of stability of Fe/N/C electrocatalysts used to reduce oxygen at the cathode of PEM fuel cells?[J]. Nano Energy, 2016, 29: 111-125.

[21] Zhang G X, Wei Q L, Yang X H, Tavares A C, Sun S H. RRDE experiments on noble-metal and noble-metal-free catalysts: Impact of loading on the activity and selectivity of oxygen reduction reaction in alkaline solution[J]. Appl. Catal. B Environ., 2017, 206: 115-126.

[22] Kresse G, Hafner J. Ab initio molecular dynamics for liquid metals[J]. Phys. Rev. B, 1993, 47(1): 558-561.

[23] Kresse G, Furthmü ller J. Efficiency of ab-initio total energy calculations for metals and semiconductors using a plane-wave basis set[J]. Comput. Mater. Sci., 1996, 6(1): 15-50.

[24] Blöchl P E. Projector augmented-wave method[J]. Phys. Rev. B, 1994, 50(24): 17953-17979.

[25] Kresse G, Joubert D. From ultrasoft pseudopotentials to the projector augmented-wave method[J]. Phys. Rev. B, 1999, 59(3): 1758-1775.

[26] Hammer B, Hansen L B, Nørskov J K. Improved adsorption energetics within density-functional theory using revised Perdew-Burke-Ernzerhof functionals[J]. Phys. Rev. B, 1999, 59(11): 7413-7421.

[27] Monkhorst H J, Pack J D. Special points for Brillouin-zone integrations[J]. Phys. Rev. B, 1976, 13(12): 5188-5192.

[28] Van Den Bossche M, Skú lason E, Rose-Petruck C, Jónsson H. Assessment of constant-potential implicit solvation calculations of electrochemical energy barriers for H_2 evolution on Pt[J]. J. Phys. Chem. C, 2019, 123(7): 4116-4124.

[29] Zhang Q, Asthagiri A. Solvation effects on DFT predictions of ORR activity on metal surfaces[J]. Catal. Today, 2019, 323: 35-43.

[30] Liu S Z, White M G, Liu P. Mechanism of oxygen reduction reaction on Pt(111) in alkaline solution: Importance of chemisorbed water on surface[J]. J. Phys. Chem. C, 2016, 120(28): 15288-15298.

[31] Ogasawara H, Brena B, Nordlund D, Nyberg M, Pelmenschikov A, Pettersson L G M, Nilsson A. Structure and bonding of water on Pt(111)[J]. Phys. Rev. Lett., 2002, 89(27): 276102.

[32] Liu K X, Qiao Z, Hwang S, Liu Z Y, Zhang H G, Su D, Xu H, Wu G, Wang G F. Mn- and N- doped carbon as promising catalysts for oxygen reduction reaction: Theoretical prediction and experimental validation[J]. Appl. Catal. B - Environ., 2019, 243: 195-203.

[33] Mathew K, Sundararaman R, Letchworth-Weaver K, Arias T A, Hennig R G. Implicit solvation model for density-functional study of nanocrystal surfaces and reaction pathways[J]. J. Chem. Phys., 2014, 140(8): 084106.

[34] Petrosyan S A, Rigos A A, Arias T A. Joint density-functional theory: *Ab initio* study of Cr_2O_3 surface chemistry in solution[J]. J. Phys. Chem. B, 2005, 109(32): 15436-15444.

[35] Valter M, Wickman B, Hellman A. Solvent effects for methanol electrooxidation on gold[J]. J. Phys. Chem. C, 2021, 125(2): 1355-1360.

[36] Gauthier J A, Dickens C F, Heenen H H, Vijay S, Ringe S, Chan K. Unified approach to implicit and explicit solvent simulations of electrochemical reaction energetics [J]. J. Chem. Theory Comput., 2019, 15(12): 6895-6906.

[37] Nørskov J K, Rossmeisl J, Logadottir A, Lindqvist L, Kitchin J R, Bligaard T, Jónsson H. Origin of the overpotential for oxygen reduction at a fuel-cell cathode[J]. J. Phys. Chem. B, 2004, 108(46): 17886-17892.

[38] Henkelman G, Jónsson H. Improved tangent estimate in the nudged elastic band method for finding minimum energy paths and saddle points[J]. J. Chem. Phys., 2000, 113(22): 9978-9985.

[39] Henkelman G, Uberuaga B P, Jónsson H. A climbing image nudged elastic band method for finding saddle points and minimum energy paths[J]. J. Chem. Phys., 2000, 113(22): 9901-9904.

[40] Sheppard D, Terrell R, Henkelman G. Optimization methods for finding minimum energy paths[J]. J. Chem. Phys., 2008, 128(13): 134106.

[41] Chen S Q, Zhang N J, Villarrubia C W N, Huang X, Xie L, Wang X Y, Kong X D, Xu H, Wu G, Zeng J, Wang H L. Single Fe atoms anchored by short-range ordered nanographene boost oxygen reduction reaction in acidic media[J]. Nano Energy, 2019, 66: 104164.

[42] Liu K X, Kattel S, Mao V, Wang G F. Electrochemical and computational study of oxygen reduction reaction on nonprecious transition metal/nitrogen doped carbon

nanofibers in acid medium[J]. J. Phys. Chem. C, 2016, 120 (3): 1586-1596.

[43] Filhol J S, Neurock M. Elucidation of the electrochemical activation of water over Pd by first principles[J]. Angew. Chem. Int. Ed., 2006, 45(3): 402-406.

[44] Yeh K Y, Janik M J. Density functional theory-based electrochemical models for the oxygen reduction reaction: Comparison of modeling approaches for electric field and solvent effects[J]. J. Comput. Chem., 2011, 32 (16): 3399-3408.

酸性和碱性溶液中金属氮碳材料氧还原和氢析出反应的理论研究

秦雪苹[1*],朱尚乾[1],张露露[1],孙书会[2],邵敏华[1*]

(1.化工与生物工程系,香港科技大学,香港 999077; 2. 能源材料与电信研究中心,魁北克 加拿大)

摘要: 单原子催化剂(SAC)由于其低成本和在各种电催化反应中潜在的高催化活性而被认为是铂族金属的有前景的替代材料,但仍然缺乏对不同金属氮碳材料催化剂之间活性差异的原子机理的理解。在此,通过实验和理论研究相结合,研究了非贵金属氮碳材料(Me-N-C,Me = Fe 和 Co)作为模型催化剂,以探索在普遍的 pH 值下氧还原反应(ORR)和氢析出反应(HER)的催化活性以及相对应的反应机理。原子理论模拟表明,Fe-N-C 具有比 Co-N-C 高的 ORR 活性,这是因为其速率决定步骤的反应势垒较低,而 HER 的活性趋势却相反。我们的模拟结果与实验观察结果一致。

关键词: 氧气还原反应;氢气析出反应;电催化剂;单原子催化剂;理论计算